DØ Note 5427-CONF

Version: 3.4

Search for GMSB in diphoton final states by D0 at $\sqrt{s} = 1.96$ TeV

The DØ Collaboration
URL http://www-d0.fnal.gov
(Dated: July 27, 2007)

We report results of a search for Supersymmetry (SUSY) with gauge-mediated breaking in diphoton events using 1100 ± 70 pb^{-1} of data collected by the D0 experiment at the Fermilab Tevatron Collider in 2002–2006. No excess of events above the standard model background is found. We set the most stringent limits for a standard benchmark model on the lightest neutralino and chargino mass of about 126 and 231 GeV, respectively, at the 95% C.L.

PACS numbers: 14.80.Ly, 12.60.Jv, 13.85.Rm

I. INTRODUCTION

Low-scale SUSY is one of the most promising solutions to the hierarchy problem associated with the large disparity between electroweak and Planck scales. It stabilizes the Higgs boson mass and postulates that for each known particle there exists a superpartner. Bosons have fermion superpartners, and vice versa. None of the superpartners have been observed, so superpartner masses must be much larger than that of their partners, *i.e.*, SUSY is a broken symmetry. Experimental signatures of supersymmetry are determined by the manner and scale of its breaking. In models with gauge-mediated supersymmetry breaking (GMSB) [1, 2] it is achieved by the introduction of new chiral supermultiplets, called messengers, which couple to the ultimate source of supersymmetry breaking, and also to the SUSY particles. At colliders, assuming R-parity conservation [3], superpartners are produced in pairs ($\chi_1^+\chi_1^-$ and $\chi_1^\pm\chi_2^0$ production dominates in most cases) and then each decays to the next-to-lightest SUSY particle (NLSP), which can be either a neutralino or a slepton. In the former case, which is considered in this note, the NLSP decays into a photon and a gravitino (the lightest superpartner in GMSB SUSY models, with mass less than ~ 1 keV) which is stable and escapes detection, creating an imbalance of transverse energy in the event. Therefore, the GMSB SUSY final state signature can be two energetic photons and large missing transverse energy ($\not\!\!E_T$). The differences in event kinematics between particular GMSB SUSY models result in slightly different experimental sensitivities [1], so to obtain quantitative results we consider a model referred to as "Snowmass Slope SPS 8" [4]. This model has only one dimensioned parameter: an energy scale Λ, that determines the effective scale of SUSY breaking. The minimal GMSB parameters correspond to a messenger mass $M_m = 2\Lambda$, the number of messengers $N_5 = 1$, the ratio of the vacuum expectation values of the two Higgs fields $\tan\beta = 15$, and the sign of the Higgsino mass term $\mu > 0$. The neutralino lifetime is not fixed in the model. For this analysis it is assumed to be short enough to result in decays with prompt photons.

GMSB SUSY was searched for by the CERN LEP collaborations [5] and at the Tevatron in both Run I [6] and early in Run II [7, 8]. The early Run II limits from CDF and D0 for the SPS 8 are combined [9] to give $\Lambda > 84.6$ TeV, which corresponds to the most stringent limit on the chargino mass of 209 GeV.

This analysis is an update of that described in Ref. [7], using about three times more data, using improved photon identification with (i) an electromagnetic (EM) cluster pointing algorithm, which allows prediction of the vertex position of the photon with a resolution of about 2 cm along the z-axis, effectively eliminating the major instrumental background associated with mis-reconstruction of the primary interaction vertex and (ii) an improved anti-track requirement that effectively suppresses sources of background with electrons in final state. We also use an improved likelihood fitter [10] to set limits on the scale Λ of gauge-mediated breaking.

II. DATA

The data used in this analysis were recorded by the D0 detector [11]. The main components of the detector are an inner tracker, liquid-argon/uranium calorimeters, and a muon spectrometer. The inner tracker consists of a silicon microstrip and central scintillating fiber trackers located in a 2 T superconducting solenoidal magnet, providing measurements up to pseudorapidities of $|\eta| \approx 3.0$ and $|\eta| \approx 1.8$, respectively. The calorimeters are finely segmented and consist of a central section (CC) covering $|\eta| < 1.2$, and two endcap calorimeters extending coverage to $|\eta| \approx 4$, all housed in separate cryostats [12]. The electromagnetic section of the calorimeter has four longitudinal layers and transverse segmentation of 0.1×0.1 in $\eta - \phi$ space (where ϕ is the azimuthal angle), except in the third layer, where it is 0.05×0.05. The central preshower system serves as a tracker by providing precision position measurements. It is placed between the solenoid and the calorimeter cryostat and provides coverage in the central region with $|\eta| \approx 1.2$. The matching resolution between CPS cluster and calorimeter EM cluster is about 0.01×0.01 in $\eta - \phi$ space which allows a precise measurement of the origin of the EM particle. The data for this study was collected between 2002 and summer 2006, using inclusive single EM triggers that are almost 100% efficient to select signal data. The integrated luminosity [13] of the sample is 1100 ± 70 pb^{-1}.

III. EVENT SELECTION

Photons and electrons are identified based on reconstructed EM clusters using calorimetric information and further classified into electron and photon candidates, based on tracking information. The EM clusters are selected from calorimeter clusters using the Simple Cone method (of radius $\mathcal{R} = \sqrt{\Delta\eta^2 + \Delta\phi^2} = 0.4$) by requiring that (i) at least 90% of the energy be deposited in the EM section of the calorimeter, (ii) the calorimeter isolation variable (I) be less than 0.15, where $I = [E_{tot}(0.4) - E_{EM}(0.2)]/E_{EM}(0.2)$, where $E_{tot}(0.4)$ is the total shower energy in a cone of radius $\mathcal{R} = 0.4$, and $E_{EM}(0.2)$ is the EM energy in a cone $\mathcal{R} = 0.2$, (iii) the transverse energy-weighted width of the

EM cluster in the EM shower maximum must be smaller than 0.04 rad, and (iv) the scalar sum of the transverse momentum (p_T) of all tracks originating from the primary vertex in an annulus of $0.05 < \mathcal{R} < 0.4$ around the cluster be less than 2 GeV/c. The EM cluster is further defined as an electron candidate if it is spatially matched to activity in the tracker, and as a photon candidate otherwise. The tracker activity can be either a reconstructed track or a density of hits in the silicon microstrip and central fiber trackers consistent with a charged track, i.e., an electron. The latter requirement allows for increasing electron track-matching efficiency, measured in $Z \rightarrow ee$ data, from $(93.0 \pm 0.1)\%$ to about $(98.6 \pm 0.1)\%$ by identifying electrons with lost tracks due to hard bremsstrahlung and/or inefficiency of inner trackers. This effectively reduces electron backgrounds to photon identification by a factor of 7, while keeping the efficiency of anti-track activity requirement high. We measure that $(91 \pm 3)\%$ of photon candidates in $Z \rightarrow ee\gamma$ data satisfy the anti-track activity requirement. Jets are reconstructed using the iterative, midpoint cone algorithm [14] with a cone size of $\mathcal{R} = 0.5$. $\not\!\!E_T$ is determined from the energy deposited in the calorimeter for $|\eta| < 4$ and is corrected for EM and jet energy scales.

We select $\gamma\gamma$ candidates by requiring events to have two photon candidates each with transverse energy $E_T > 25$ GeV identified in the central calorimeter ($|\eta| < 1.1$). We require that at least one of the photon candidates is matched to a CPS cluster, and that the primary vertex is consistent with the photon candidate vertex obtained from CPS-EM pointing algorithm. The accuracy of the determination of the photon vertex is measured using final state radiation photons in $Z \rightarrow ee\gamma$ data sample and found to be 2.3 ± 0.3 cm. The requirement of consistency between the photon and primary vertices ensures correct calculation of the transverse energies and tracking isolation requirements. The accuracy of primary vertex association is studied in GMSB SUSY Monte Carlo simulated events, where the primary vertex is identified correctly in $(98.5 \pm 0.1)\%$, while the photon vertex matched the primary vertex in $(95.8 \pm 0.1)\%$.

To reduce potential bias to the $\not\!\!E_T$ measurement due to mis-measured jet transverse momentum, we also require that the jet with highest value of E_T (if jets are present in the event) be separated from $\not\!\!E_T$ in azimuthal angle by no more than 2.5 radians. This selection yields 2341 events ($\gamma\gamma$ sample).

IV. BACKGROUNDS

All instrumental backgrounds arise from standard model processes with either genuine $\not\!\!E_T$ ($W\gamma$, $W + jet$, and $t\bar{t}$ production) or without inherent $\not\!\!E_T$ (direct photon, multi-jet, $Z \rightarrow ee$ production). All these backgrounds are measured in data.

The former source always has an electron in the final state which is misidentified as a photon. The contribution of this background to the data $\not\!\!E_T$ distribution can be estimated using an $e\gamma$ sample (selected by requiring an electron and a photon candidates and using the same kinematical requirements as for the $\gamma\gamma$ sample) scaled by the probability of an electron-photon misidentification which is measured using $Z \rightarrow ee$ data. First, the $\not\!\!E_T$ distribution in the $e\gamma$ sample needs to be corrected for the contributions from the events with no real $\not\!\!E_T$: Z/γ^* (Drell-Yan) and multi-jet and γ+jet events with mis-identified electrons. The contribution from the Drell-Yan is taken into account by obtaining the $\not\!\!E_T$ distribution for the ee sample (selected by requiring two electron candidates and applying the same kinematical requirement as that for the $\gamma\gamma$ sample) which is dominated by the Drell-Yan events. The Drell-Yan $\not\!\!E_T$ distribution is further normalized to the number of Z boson events in the $e\gamma$ sample (the latter is determined by fitting the $e\gamma$ invariant mass spectrum to the Z boson mass peak).

The contribution from the multi-jet processes is estimated from a data sample (referred to as QCD sample) selected by requiring 2 EM clusters that (a) satisfy all the kinematic selection used to select $\gamma\gamma$ sample and (b) satisfy all the photon identification criteria but fail the shower shape requirement. The $\not\!\!E_T$ distribution in the QCD sample is normalized to the number of the events in the $e\gamma$ sample with $\not\!\!E_T < 12$ GeV after subtraction of the Drell-Yan contribution as determined above. Expected number of $W\gamma$, $W + jet$, and $t\bar{t}$ events with $\not\!\!E_T < 12$ GeV is negligible.

After the Drell-Yan and multi-jet contributions to $e\gamma$ sample are subtracted, the resulting $\not\!\!E_T$ distribution is scaled by $(1 - \epsilon_{trk})/\epsilon_{trk}$, where ϵ_{trk} is the efficiency of the track-matching requirement to obtain the estimate of $\not\!\!E_T$ distribution for the background with genuine $\not\!\!E_T$.

The background from events with no inherent $\not\!\!E_T$ is divided into multi-jet events with two real isolated photons and events where one or both photons are mis-identified jets. Since $\not\!\!E_T$ resolution for both sources is dominated by the photon energy resolution, the $\not\!\!E_T$ distribution for the two sources are very similar. However, mis-identified jets have a different energy response compared with that of real photons which leads to a slight difference in shapes of $\not\!\!E_T$ distributions. For the real di-photons, the $\not\!\!E_T$ is assumed to have the same shape as that for the Drell-Yan events. For misidentified jets, the shape of $\not\!\!E_T$ distribution is taken from the QCD sample. Relative normalization of the two sources is obtained using a fit to the $\not\!\!E_T$ distribution in the $\gamma\gamma$ sample. We have checked that the fit is robust with respect to possible signal contribution, and have cross-checked using a method that estimates $\gamma\gamma$ sample purity using measured shower shape in the preshower. The relative fraction of di-photons is $60 \pm 20\%$ and its error is propagated into the limit setting as one of the systematic errors. Absolute normalization of $\not\!\!E_T$ distributions from both sources

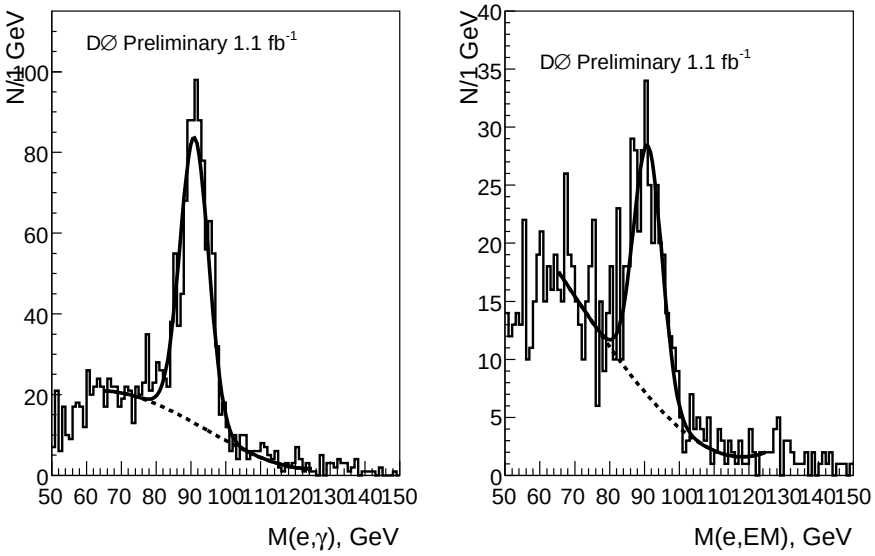

FIG. 1: Fit of di-EM invariant mass to gaussian and polynomial in $e\gamma$ (left) and eh (right) samples (see text for explanation).

determined so that the number of events for $\not\!\!E_T < 12$ GeV matches $\gamma\gamma$ sample.

We also perform a cross-check to verify that the $\not\!\!E_T$ distribution due to processes with real $\not\!\!E_T$ can be described by $W\gamma$ and $W + jet$ processes. The $\not\!\!E_T$ distribution from $W\gamma$ processes is obtained from a standard Pythia $W\gamma$ Monte Carlo simulation, and the overall normalization was obtained from the luminosity. The $W + jet$ background is estimated by selecting an eh sample by requiring events to have an electron candidate and an EM object that passed the photon identification criteria with an inverted shower shape requirement. The $\not\!\!E_T$ distribution in the eh sample is composed of $\not\!\!E_T$ contributions from Drell-Yan, QCD, and $W + jet$ processes. By fitting the di-EM invariant mass (see the right plot in Figure 1) we determine the overall normalization for the Drell-Yan $\not\!\!E_T$ contribution. By normalizing the misidentified jet $\not\!\!E_T$ distribution to the eh events with $\not\!\!E_T < 12$ GeV after subtraction of the Drell-Yan $\not\!\!E_T$ contribution, we determine the contribution from misidentified jets. Thus, we obtain the $W + jet$ $\not\!\!E_T$ distribution by subtracting $\not\!\!E_T$ contributions due to QCD and Drell-Yan processes from that in the eh sample. The resulting $W + jet$ $\not\!\!E_T$ distribution is further modified by the misidentification rate (obtained by dividing the QCD $\not\!\!E_T$ distributions in $e\gamma$ and eh samples) to be compared with the $\not\!\!E_T$ distribution in the $e\gamma$ sample. The agreement of the predicted and observed $\not\!\!E_T$ distribution in $e\gamma$ sample is very good and is illustrated in Figure 2.

The largest contributions from physics backgrounds arise from $Z\gamma\gamma \to \nu\nu\gamma\gamma$ and $W\gamma\gamma \to \ell\gamma\gamma\nu$ processes. Contributions from these backgrounds were estimated to be 0.15 ± 0.06 and 0.10 ± 0.04 events, respectively, using the CompHep [15] Monte Carlo simulation, cross-checked with MADGRAPH [16]. The contribution of these backgrounds to the $\gamma\gamma$ $\not\!\!E_T$ distribution is taken from Monte Carlo simulation with number of events normalized to the integrated luminosity of the data sample.

V. RESULTS

The $\not\!\!E_T$ distributions for the $\gamma\gamma$ sample, contributions from physics background ($W/Z + \gamma\gamma$), instrumental background with genuine $\not\!\!E_T$ (processes with misidentified electrons), and no inherent $\not\!\!E_T$ ($\gamma\gamma$ and multi-jet) is given in Fig. 3. We also illustrate the expected $\not\!\!E_T$ distribution for the GMSB SUSY signal for two different values of Λ. The number of observed events as well as expected background and GMSB SUSY signal for two values of Λ for $\not\!\!E_T > 30$ and 60 GeV are given in Table I.

VI. SIGNAL SIMULATION

The expected signal efficiency is estimated from GMSB SUSY Monte Carlo simulation generated for several points on the Snowmass Slope (see Table II), covering the neutralino mass range from 170 GeV to 280 GeV. We consider

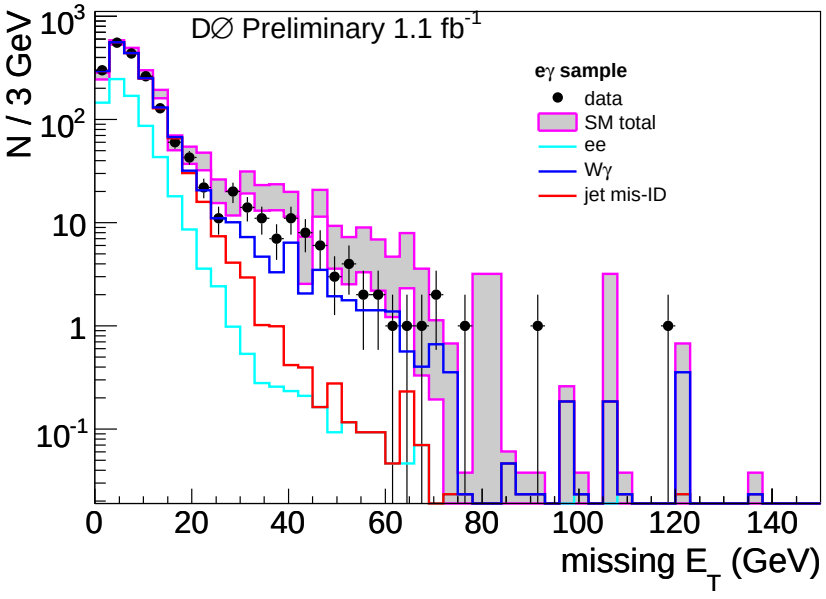

FIG. 2: The $\not\!\!E_T$ distribution in the $e\gamma$ sample (black circles) compared with the standard model prediction (magenta histogram, shaded area indicates an uncertainty in prediction).

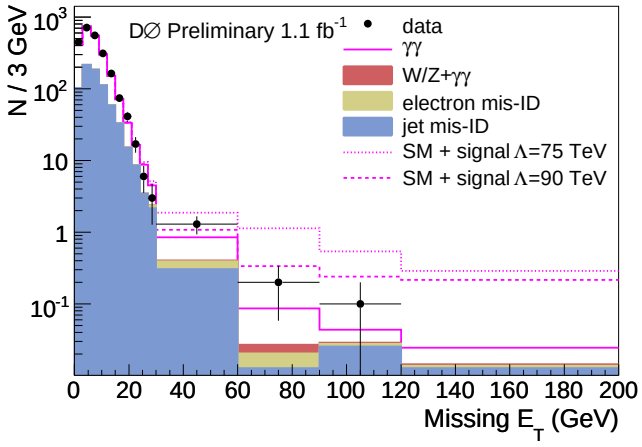

FIG. 3: The $\not\!\!E_T$ distribution in $\gamma\gamma$ data with $W/Z + \gamma\gamma$ background (brown filled histogram), instrumental background with no genuine $\not\!\!E_T$: $\gamma\gamma$ (red histogram) and multi-jet (blue filled histogram), and background from processes with genuine $\not\!\!E_T$ and misidentified electron (pale green histogram). Expected $\not\!\!E_T$ distribution for GMSB SUSY signal with $\Lambda = 75$ TeV and 90 TeV are presented as dotted and dashed magenta lines, respectively.

	No. background events				No. expected signal events		No. observed events
	Genuine $\not\!\!E_T$	no $\not\!\!E_T$	Physics	Total	$\Lambda = 75$ TeV	$\Lambda = 90$ TeV	
$\not\!\!E_T > 30$ GeV	0.97±0.12	9.62 ±1.12	0.19±0.07	10.8±1.1	28.3±1.0	8.7±0.3	16
$\not\!\!E_T > 60$ GeV	0.11±0.04	1.44 ±0.43	0.08±0.04	1.6±0.4	18.1±0.8	6.4±0.3	3

TABLE I: Number of background events from $W\gamma$, $W + jet$, and $t\bar{t}$ (Genuine $\not\!\!E_T$), no inherent $\not\!\!E_T$ (no $\not\!\!E_T$), $Z\gamma\gamma \to \nu\nu\gamma\gamma$ and $W\gamma\gamma \to \ell\gamma\gamma\nu$ (Physics) processes, and the total number of the expected background; number of the expected GMSB SUSY signal events for two values of Λ; and the observed number of events for $\not\!\!E_T > 30$ and 60 GeV.

Λ, TeV	$m_{\chi_1^0}$, GeV	$m_{\chi_1^+}$, GeV	σ^{LO}, fb	k-factor	Efficiency
70	93.7	168.2	215 ± 9	1.207	0.17 ± 0.03
75	101.0	182.3	148 ± 6	1.197	0.18 ± 0.03
80	108.5	198.1	97.5± 3.9	1.187	0.18 ± 0.03
85	115.8	212.0	65.4± 2.6	1.177	0.19 ± 0.03
90	123.0	225.8	41.8± 1.7	1.167	0.19 ± 0.03
95	130.2	239.7	29.5± 1.2	1.157	0.20 ± 0.03
100	137.4	253.4	20.6± 0.8	1.147	0.20 ± 0.03
105	144.5	267.0	14.4± 0.6	1.137	0.18 ± 0.03
110	151.7	280.7	10.3± 0.4	1.127	0.19 ± 0.03

TABLE II: Points on the GMSB model Snowmass slope: neutralino and chargino masses, cross sections, k-factors, and reconstruction efficiencies.

Source	Uncertainty
EM identification	10%
Signal Monte Carlo statistics	5%
Trigger efficiency	4%
Anti-track matching requirements	3%
PDF uncertainties	4%
Luminosity	6.5%

TABLE III: Sources and values of statistical and luminosity uncertainties.

all GMSB SUSY production channels although $\chi_1^+\chi_1^-$ and $\chi_1^\pm\chi_2^0$ processes dominate. We used ISAJET 7.58 [17] to determine SUSY interaction eigenstate masses and couplings. PYTHIA 6.202 [18] was used to generate the events after determining the sparticle masses, branching fractions and leading order (LO) production cross sections using CTEQ6L1 structure functions [19]. The generated events are processed through a full detector simulation and the same reconstruction code as for data. The LO signal cross sections are scaled to match the next-to-leading order (NLO) prediction using k-factor values (see Table II), extracted from Ref. [20].

We list systematic and luminosity uncertainties in Table III. The total uncertainty in background contribution is dominated by the statistical uncertainty.

VII. LIMIT SETTING AND CONCLUSIONS

As the observed number of events for all values of $\not\!\!E_T$ is in a good agreement with the standard model prediction, we conclude that there is no evidence for GMSB SUSY in data. We set limits on the production cross section by utilizing a likelihood fitter [10] that incorporates a log-likelihood ratio (LLR) test statistic method. This method utilizes binned $\not\!\!E_T$ distributions rather than a single-bin (fully-integrated) value, and therefore accounts for the shape of the distributions, leading to better sensitivity. The value of the confidence level for the signal CL_s is defined as $CL_s = CL_{s+b}/CL_b$, where CL_{s+b} and CL_b are the confidence levels for the signal plus background hypothesis and the background-only (null) hypothesis, respectively. These confidence levels are evaluated by integrating corresponding LLR distributions populated by simulating outcomes via Poisson statistics. Systematic uncertainties are treated as uncertainties on the expected numbers of signal and background events, not the outcomes of the limit calculations. This approach ensures that the uncertainties and their correlations are propagated to the outcome with their proper weights. The limits are shown in Fig. 4 together with expected signal cross sections. The observed limits are statistically compatible with the expected ones. The upper-limit on the signal cross section is below the expected value for $\Lambda < 92$ TeV, or in terms of gaugino masses, $m_{\chi 10} < 126$ GeV and $m_{\chi_1^+} < 231$ GeV. These represent the most stringent limits on this particular GMSB SUSY model to date.

VIII. ACKNOWLEDGEMENT

We thank the staffs at Fermilab and collaborating institutions, and acknowledge support from the DOE and NSF (USA); CEA and CNRS/IN2P3 (France); FASI, Rosatom and RFBR (Russia); CAPES, CNPq, FAPERJ, FAPESP and FUNDUNESP (Brazil); DAE and DST (India); Colciencias (Colombia); CONACyT (Mexico); KRF and

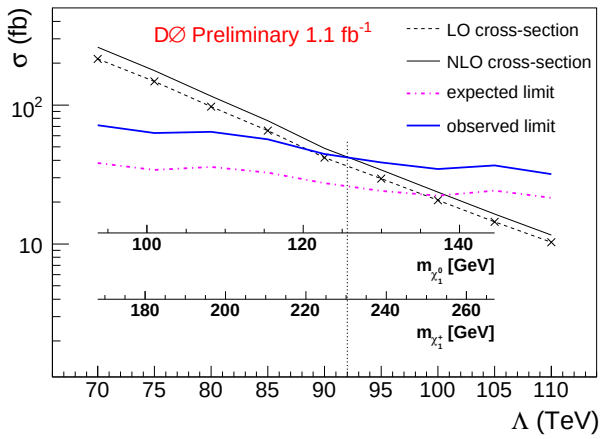

FIG. 4: Predicted cross sections for the Snowmass Slope model versus Λ in leading order (thin dashed line with crosses), multiplied by the k-factor (thin solid line). The observed and expected 95% C.L. limits are shown in solid and dash-dotted lines, respectively.

KOSEF (Korea); CONICET and UBACyT (Argentina); FOM (The Netherlands); Science and Technology Facilities Council (United Kingdom); MSMT and GACR (Czech Republic); CRC Program, CFI, NSERC and WestGrid Project (Canada); BMBF and DFG (Germany); SFI (Ireland); The Swedish Research Council (Sweden); CAS and CNSF (China); Alexander von Humboldt Foundation; and the Marie Curie Program.

[1] P. Fayet, Phys. Lett. B **70**, 461 (1977); *ibid.* **86**, 272 (1979); *ibid.* **175**, 471 (1986).
[2] M. Dine, A. E. Nelson, Y. Nir and Y. Shirman, Phys. Rev. D **53**, 2658 (1996); H. Baer, M. Brhlik, C. H. Chen and X. Tata, Phys. Rev. D **55**, 4463 (1997); H. Baer, P. G. Mercadante, X. Tata and Y. L. Wang, Phys. Rev. D **60**, 055001 (1999); S. Dimopoulos, S. Thomas and J. D. Wells, Nucl. Phys. B **488**, 39 (1997); J. R. Ellis, J. L. Lopez and D. V. Nanopoulos, Phys. Lett. B **394**, 354 (1997); see also a review by G. F. Giudice and R. Rattazzi, "Gauge-Mediated Supersymmetry Breaking" in G. L. Kane: *Perspectives on Supersymmetry*, World Scientific, Singapore (1998), p. 355-377, and references therein.
[3] G.R. Farrar and P. Fayet, Phys. Lett. **B79** (1978) 442.
[4] S.P. Martin, `http://zippy.physics.niu.edu/modellineE.html`; S.P. Martin, S. Moretti, J.M. Qian, and G.W. Wilson, "Direct Investigation of Supersymmetry: Subgroup summary report," in *Proceedings of the APS/DPF/DPB Summer Study on the Future of Particle Physics (Snowmass 2001),* edited by N. Graf, eConf **C010630**, p. 346 (2001); B.C. Allanach *et al.*, Eur. Phys. J. C **25**, 113 (2002).
[5] LEP SUSY Working Group, ALEPH, DELPHI, L3, and OPAL Collaborations, LEPSUSYWG/04-09.1 (`http://lepsusy.web.cern.ch`).
[6] B. Abbott *et al.*, Phys. Rev. Lett. **80**, 442 (1998); F. Abe *et al.*, Phys. Rev. D **59**, 092002 (1999).
[7] V. Abazov *et al.*, Phys. Rev. Lett. **94**, 041801 (2005).
[8] D. Acosta *et al.*, Phys. Rev. D **71**, 031104(R) (2005).
[9] V. Buescher *et al.*, hep-ex/0504004.
[10] W. Fisher, FERMILAB-TM-2386-E; T. Junk, Nucl. Instrum. Meth. A **434**, 435-443 (1999); A. Read, "Modified Frequentist Analysis of Search Results (The CLs Method)", CERN 2000-005 (30 May 2000).
[11] V.M. Abazov *et al.* (D0 Collaboration), "The upgraded DØ detector," Nucl. Instrum. Methods Phys. Res. A **565**, 463 (2006).
[12] S. Abachi, *et al.* (D0 Collaboration), Nucl. Instrum. Methods Phys. Res. A **338**, 185 (1994).
[13] T. Andeen *et. al.*, FERMILAB-TM-2365-E (2006).
[14] G.C. Blazey *et al.*, in *Proceedings of the Workshop: QCD and Weak Boson Physics in Run II,* edited by U. Baur, R.K. Ellis, and D. Zeppenfeld, Fermilab-Pub-00/297 (2000).
[15] A. Pukhov *et al.*, Preprint INP MSU 98-41/542; hep-ph/9908288.
[16] F. Maltoni and T. Stelzer, JHEP **0302**, 027 (2003); hep-ph/0208156.
[17] F.E. Paige, S.D. Protopescu, H. Baer, and X. Tata, hep-ph/0312045.
[18] T. Sjöstrand *et al.*, Comput. Phys. Commun. **135**, 238 (2001).
[19] J. Pumplin *et al.*, JHEP **0207** 012 (2002) and D. Stump *et al.*, JHEP **0310** 046 (2003).
[20] W. Beenakker *et al.*, Phys. Rev. Lett. **83**, 3780 (1999).